Biosensors and Bioelectronics 141 (2019) 111351

Contents lists available at ScienceDirect

Biosensors and Bioelectronics

journal homepage: www.elsevier.com/locate/bios

A sensitive label-free impedimetric DNA biosensor based on silsesquioxane-functionalized gold nanoparticles for Zika Virus detection

Marines Steinmetz, Dhésmon Lima, Adriano Gonçalves Viana, Sérgio Toshio Fujiwara, Christiana Andrade Pessôa, Rafael Mazer Etto, Karen Wohnrath*

Department of Chemistry, Universidade Estadual de Ponta Grossa, Av. General Carlos Cavalcanti, 4748, 84030-900, Ponta Grossa, Paraná, Brazil

ARTICLE INFO

Keywords:
ZIKV diagnosis
Impedimetric biosensor
Gold nanoparticles
Silsesquioxane

ABSTRACT

Zika virus (ZIKV) has recently become a global health challenge due to its rapid geographical expansion, since it is associated with serious neurological anomalies such as Guillain-Barré syndrome and microcephaly. Currently, the techniques for ZIKV diagnosis require labor-intensive, expensive and lengthy tests using sophisticated equipment. Moreover, false-positive or false-negative results can occur. In the present work, a DNA biosensor to detect ZIKV in real human serum samples was developed using an oxidized glassy carbon electrode (ox-GCE) modified with silsesquioxane-functionalized gold nanoparticles (AuNPs-SiPy). This nanohybrid was characterized by UV-Vis, FTIR and Raman spectroscopies, DLS, and XRD. The conditions for the immobilization of a ZIKV ssDNA probe on the electrode surface (ox-GCE-[AuNPs-SiPy]) were optimized by univariate and multivariate analysis. The optimized biosensor was characterized by CV, EIS and AFM experiments. The ZIKV target recognition was based on the variation of the charge transfer resistance (ΔR_{ct}) of the redox marker ($[Fe(CN)_6]^{3-/4-}$) used and the roughness (R_q) of the electrode surface. The proposed biosensor presented a LOD of 0.82 pmol L^{-1}, with a linear range of 1.0 x10^{-12} – 1.0 x10^{-6} mol L^{-1}. Moreover, the reported device showed a suitable stability and satisfactory sensitivity and selectivity to quantify ZIKV in human serum samples, which suggests its promising clinical applications for the early diagnosis of ZIKV-associated pathologies.

1. Introduction

ZIKV is a mosquito-borne *Flavivirus* first identified in the Zika Forest of Uganda in 1947. Since its discovery, the virus has spread and undergone mutations which recently led to significantly outbreaks, becoming a global health challenge (Musso and Gubler, 2016). Infections reached Micronesia (2007), French Polynesian (2013) and countries from the Americas and Asia (2015/2016). In 2015, the Brazilian Ministry of Health estimated that up to 1.3 million suspected cases had occurred (Petersen et al., 2016). In 2016, the World Health Organization declared ZIKV a public health emergency of international concern (Dowall et al., 2017). The long-term effects of ZIKV include several brain abnormalities in newborns, especially microcephaly, and may trigger Guillain-Barré syndrome, a severe autoimmune disease, in adults (Araujo et al., 2016; Amorim, 2019).

Correct diagnosis of ZIKV-infected individuals is challenging because its clinical symptoms are usually non-specific (~80%) and similar to other flaviviruses such as Dengue and Chikungunya (Martinez et al., 2019). Techniques employed for the detection of ZIKV include quantitative-reverse-transcription/polymerase-chain-reaction (qRT-PCR), loop-mediated isothermal amplification (LAMP) and Zika IgM antibody capture enzyme-linked immunosorbent assay (ELISA). These methods are usually lengthy, require professional handling, use expensive equipment and resources and can also give false positive or negative diagnoses (Singh et al., 2018). Therefore, the development of more sensitive, accurate, fast and affordable methods to screen for ZIKV epidemics is highly desirable. Some biosensing approaches have already been reported in the literature based on ribonucleic acid (RNA) (Pardee et al., 2016) and antigens/antibodies (AG/AB) in electrochemical platforms constituted by graphene (Afsahi et al., 2018) and interdigitated electrodes (Kaushik et al., 2018) with LOD values in the range of 2.8 x 10^{-15} – 0.4 x 10^{-9} mol L^{-1} for the detection of ZIKV. Additionally, Tancharoen et al. (2018) used the entire virus structure immobilized on a gold interdigitated electrode modified with graphene oxide and a gel polymer (IDE-GoxPol), with a LOD of 1.0 x 10^{-20} mol L^{-1} (Tancharoen et al., 2018). More recently, it was published the first biosensor based on the immobilization of synthetic ZIKV DNA oligonucleotide on a gold-modified polyethylene terephthalate (PET)

* Corresponding author.
E-mail address: karen.woh@gmail.com (K. Wohnrath).

https://doi.org/10.1016/j.bios.2019.111351
Received 26 February 2019; Received in revised form 22 May 2019; Accepted 23 May 2019
Available online 27 May 2019
0956-5663/

electrode, which reached a LOD of 25 x 10^{-9} mol L^{-1} (Faria and Zucolotto, 2019).

DNA electrochemical biosensors based on gold nanoparticles (AuNPs) have been recently developed as alternatives for simple diagnosis of infectious agents (Huang et al., 2017). The incorporation of AuNPs in the biosensing platform can provide an enhancement of the device's response, due to interesting properties such as high electrical conductivity and high surface area. (Alex and Tiwari, 2015; Saha et al., 2012). Furthermore, AuNPs can assist the immobilization of biomolecules on the electrodic surface, enhancing the sensitivity and robustness of the device towards the analyte detection (Chao et al., 2016), which is due to the increased amount of immobilized DNA and the highly selective hybridization (Cai et al., 2001).

Thiol-gold bonds are effective to adhere oligonucleotides to nanoparticle surfaces, yielding biosensors with molecular organization, ultrasensitive performance and stability (Austin et al., 2014; Rafique et al., 2018). Mashhadizadeh and Talemi (2016) have showed the immobilization of a thiolate DNA probe on a carbon paste electrode modified with 3-(trimetilsilsesquioxane)-1-propanethiol and AuNPs. The Au-S covalent bonds provided a selective and reproducible sensor for the detection of Hepatitis B virus in urine and plasma samples, with a LOD of 3.1 x 10^{-13} mol L^{-1}. Similarly, a platform based on the coelectrodeposition of AuNPs and reduced graphene oxide (rGO) on a glassy carbon electrode (GCE) was used to immobilize thiolate DNA probes, presenting a LOD of 3.9×10^{-14} g mL^{-1} (Kumarasamy et al., 2018) to the determination of DNA hybridization with potential application in cancer diagnostics.

In spite of their interesting features, nanoparticles are usually thermodynamic unstable. Therefore, it is necessary the use of stabilizing agents in order to obtain stable nanohybrids, with a small tendency to undergo coalescence (Mossanha et al., 2017). Silsesquioxane polyelectrolytes are a class of silicon polymers which present positive charges on their polymeric structures, showing the ability to support and stabilize AuNPs (Da Silva et al., 2014). Calaça et al. (2017) and De Menezes et al. (2012) reported the use of 3-*n*-propylpyridinium silsesquioxane polymer (SiPy) for the synthesis of AuNPs. According to the authors, the polymeric chains allowed the adsorption of $AuCl_4^-$ complex precursor, enabling the formation of AuNPs with diameters of 11.0 and 6.1 nm, respectively.

To the best of our knowledge, only one sensor containing DNA for ZIKV have been previously reported. In this sense, the main objective of this work is to develop a new label-free DNA biosensor for the detection of ZIKV, based on a platform constituted by SiPy-stabilized AuNPs (AuNPs-SiPy) employing an oxidized GCE as transducer.

2. Experimental section

2.1. Reagents and DNA oligonucleotides

All reagents used in this work were of analytical grade and used without previous purification. $K_4[Fe(CN)_6].3H_2O$, $K_3[Fe(CN)_6]$ and $HAuCl_4.3H_2O$ were purchased from Sigma-Aldrich. SiPy was synthetized as described in the literature (Alfaya et al., 1998). Phosphate buffered saline solution (PBS) was prepared at pH 7.4 by using 0.15 mol L^{-1} NaCl, 7.2 mmol L^{-1} Na_2HPO_4, and 2.8 mmol L^{-1} NaH_2PO_4. HPLC-purified DNA oligonucleotides were synthesized and purchased from Integrated DNA Technologies (IDT, Inc., Coralville, IA). The ssDNA oligonucleotides used in this work were: (i) ZIKV1, a thiolate ZIKV-specific probe with the following sequence: 5′-ThioMC6-D-AGCC ATGACCGACACCACACCGT-3′ (Zhang et al., 2016; Deng et al., 2017); (ii) ZIKV2, a sulfur-free target oligonucleotide complementary to ZIKV1; and (iii) No-ZIKV2, a sulfur-free oligonucleotide non-complementary to ZIKV1 (5′-GAGAGGTACCCGAACTGCAAC-3′) used as negative control and to demonstrate that nonthiolate DNA does not interact with the AuNPs in this DNA biosensor approach. All solutions were made with ultra high purity sterile water (18.2 MΩ cm, Milli-Q). Oligonucleotides solutions were stored at -20 °C. Human serum used as real matrix were obtained from a healthy subject in accordance with institutional ethics policies. The study was approved by the Research Ethics Committee (CAAE: 62060616.2.0000.0105).

2.2. Synthesis and characterization methods of AuNPs-SiPy nanohybrid

The AuNPs were synthetized according to an established procedure from the literature (Calaça et al., 2017). The obtained nanohybrid was characterized by UV-Vis spectroscopy (Cary 50 Varian spectrophotometer), Zeta potential determination and dynamic light scattering (DLS) (Malvern NanoZ590 equipment), FTIR (Shimadzu 8400 spectrometer), Raman spectroscopy (stray Raman Bruker Senterra spectrometer) and X-ray diffractometry (XDR) analysis (Rigaku Ultima IV diffractometer). FTIR spectra were recorded in the transmittance mode in the range from 400 to 4,000 cm^{-1} (resolution: 4 cm^{-1}; number of scans: 64) by using KBr pellets containing SiPy or lyophilized AuNPs-SiPy. Raman spectra and X-ray diffractograms were taken for SiPy and AuNPs-SiPy lyophilized powders.

2.3. ZIKV DNA biosensor preparation

Glassy carbon electrodes (geometric area = 3.1 mm^2) were first polished with alumina/water slurry (0.3 μm) on a flat pad. The electrodes were then washed with ultra-pure water and sonicated in absolute ethanol for 5 min. The fabrication process of the ZIKV DNA biosensors consisted in the steps summarized in Scheme 1 (see Supplementary Material S1 for a detailed description). The obtained biosensors were designated as ox-GCE-[AuNPs-SiPy]/ZIKV1.

2.4. ZIKV biosensor optimization

The amount of AuNPs-SiPy (2, 5, 10 and 15 μL) used for the ox-GCE modification was optimized by using univariate analysis. Sequentially, the probe concentration ([ZIKV1]) and probe incubation time ($time_{inc}$) were optimized by using a multivariate approach. For this purpose, a 3^2 factorial design was employed. The studied levels of the variables were based on preliminary tests: [ZIKV1] = 1 (-1), 5.5 (0), and 10 μmol L^{-1} (+1); and probe $time_{inc}$ = 90 (-1), 120 (0), and 150 min (+1). In all hybridization assays, the temperature was kept constant at 25 °C. The evaluated response was the percent variation of the charge transfer resistance (ΔR_{ct}) in the EIS measurements, which was obtained after performing electrochemical assays with a fixed concentration of ZIKV2 (10 μmol L^{-1}). For ΔR_{ct} calculation, the following equation was used:

$$\Delta R_{ct} = \left(\frac{R_{ct\ (hib)} - R_{ct\ (bios)}}{R_{ct\ (bios)}} \right). 100\%$$

where $R_{ct\ (hib)}$ and $R_{ct\ (bios)}$ refer to the R_{ct} values obtained after and before the hybridization assay, respectively. The data processing was carried out by using *Statistica*® 13.0 software.

The hybridization temperature was finally analyzed by a univariate experiment, between 25, 37 and 50 °C. All measurements were evaluated by the obtained ΔR_{ct} value. The optimized experimental conditions were then employed to obtain analytical curves for the ZIKV2 target detection, in the range from 1 pmol L^{-1} to 1 μmol L^{-1}.

2.5. Electrochemical measurements

All electrochemical experiments were performed at room temperature, using a conventional three-electrode cell system, consisted of unmodified or modified GCE as the working electrode, Ag|AgCl as the reference electrode and a platinum spiral wire as the auxiliary electrode. CV and EIS measurements were carried out in a Multipotenciostat Autolab® MAC90149 connected to a computer with *Nova 2.1* software. 0.15 mol L^{-1} PBS buffer containing 5.0 mmol L^{-1} K_4Fe

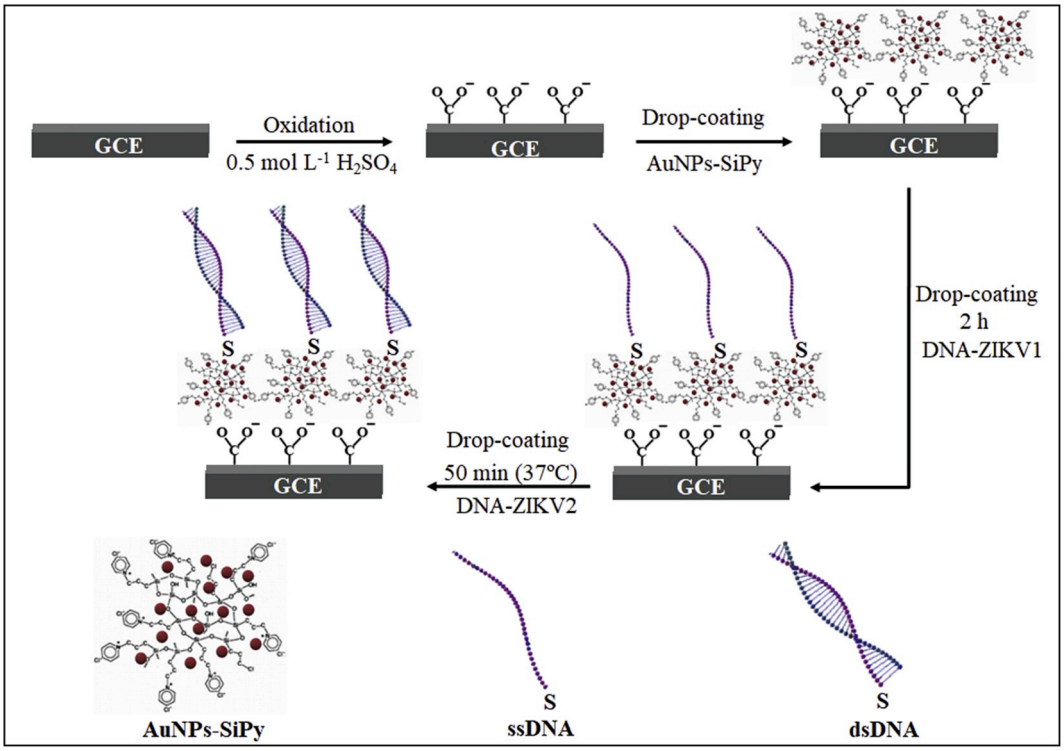

Scheme 1. Schematic representation of the stages of the ox-GCE-[AuNPs-SiPy]/ZIKV1 biosensor construction and DNA hybridization.

$(CN)_6/K_3Fe(CN)_6$ was used as supporting electrolyte, since the DNA probes used in this study were not redox labeled. Before all measurements, the electrolyte was purged for 10 min with high-purity nitrogen flow. Analytical parameters such as limit of detection (LOD) was determined for the developed biosensor following the guidelines stated by the International Union of Pure and Applied Chemistry (IUPAC) (Nic et al., 1997).

2.6. Biosensor characterization

All stages of the biosensor construction were characterized by CV, EIS and AFM. AFM images and roughness values (R_q) were obtained in a Shimadzu SPM 9600 microscope in the non-contact mode, with a Silicon SPM Sensor (Al-coating) (NANO WORD) with thickness 4 µm, length 125 µm, width 30 µm, frequency 320 Hz, and constant force of 42.0 N m^{-1}.

2.7. Real sample analysis and stability studies

Fresh human serum samples were spiked with 15 µmol L^{-1} of ZIKV2. This mixture was sequentially diluted in order to obtain target concentrations of 1,000, 1.0 and 0.01 nmol L^{-1}. The stability of the proposed biosensor was evaluated by storing three modified electrodes containing ZIKV1 (ox-GCE-[AuNPs-SiPy]/ZIKV1) at 4 °C and performing EIS measurements over a period of time (0 to 90 days) towards the specific hybridization with ZIKV2. After each experiment at 1, 2, 7, 14, 21, 28, 35, 60 and 90 days, the biosensors were cleaned and another platform was constructed at each test.

3. Results and discussion

3.1. Synthesis and characterization of AuNPs-SiPy

The formation of AuNPs was confirmed by the presence of the surface plasmon resonance band in the UV-Vis spectra of the obtained suspension. The interactions between the AuNPs and SiPy polymer was confirmed by FTIR and Raman spectroscopies. The crystallinity of both the polymer and the AuNPs-SiPy hybrid was confirmed by XRD (see Supplementary Material S2 for a detailed description).

3.2. Electrochemical characterization of GCE, ox-GCE, ox-GCE-[SiPy] and ox-GCE-[AuNPs-SiPy]

The electrochemical behavior of the AuNPs-SiPy immobilized on the ox-GCE surface was investigated by CV measurements in 0.5 mol L^{-1} H_2SO_4. An anodic and a cathodic peak were observed at 0.41 and 0.95 V (*vs.* Ag|AgCl), respectively (Fig. S3.1). According to the literature, the typical redox processes for a gold macroelectrode occur around 0.85 and 1.18 V (*vs.* Ag|AgCl). Those processes are associated with the formation of gold oxides (Au = O and O = Au–$(H_2O)_{ads}$) during the anodic scan that remain absorbed on the electrode surface and are reduced during the reverse scan (Wang et al., 2013; Burke and Nugent, 1997). The shift to lower potentials observed for the ox-GCE-[AuNPs-SiPy] suggest that the electron transfer process is easier on this surface (Saha et al., 2012). In comparison, the bare GCE, ox-GCE and ox-GCE-[SiPy] presented just the background current in the same potential range.

In order to evaluate the stability of the ox-GCE-[AuNPs-SiPy], successive potential scans between 0.2 and 1.6 V (around 22 cycles) were performed (Fig. S3.2). The obtained voltammograms revealed that the cathodic peak potential (E_{pc}) and cathodic peak current (I_{pc}) did not change significantly. Thus, one can affirm that the AuNPs-SiPy remained stable on the ox-GCE surface. When cyclic voltammograms were performed with this electrode in 0.5 mol L^{-1} PBS buffer (Fig. S3.3), no electrochemical response was observed. Hence, all further electrochemical measurements were carried out in the presence of 5.0 mmol L^{-1} $K_4[Fe(CN)_6]/K_3[Fe(CN)_6]$ as a redox marker, which is commonly used for the characterization of biosensors.

The GCE, ox-GCE, ox-GCE-[SiPy] and ox-GCE-[AuNPs-SiPy] platforms were characterized by CV and EIS measurements. Voltammograms shown in Fig. S3.4 (A) demonstrate a quasi-reversible behavior due to the electrochemical redox marker for all electrode

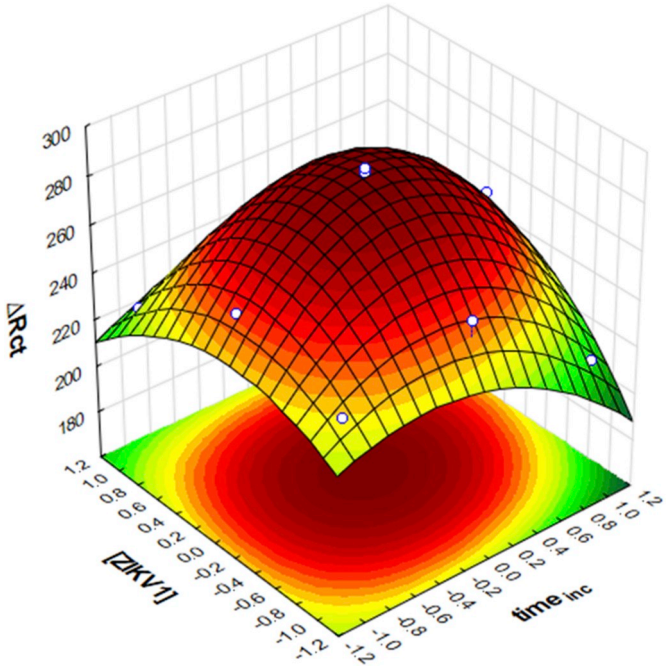

Fig. 1. Response surface plot for ΔR_{ct} as a function of [ZIKV1] and $time_{inc}$.

configurations. The Nyquist diagram (Fig. S3.4 (B)) exhibited two regions: a semicircular part, corresponding to the electron transfer-limited process and a linear segment representing the diffusional process of $[Fe(CN)_6]^{4-/3-}$ ions (Brett and Brett, 1993; Bard and Faulkner, 2001). All R_{ct} values (Table S3.1) were obtained from *Nova 2.1* software using equivalent circle analysis.

The CV for unmodified GCE showed higher current peaks (I_p), a lower peak-to-peak potential separation (ΔE_p) and a lower R_{ct} value, due to faster electron transfer kinetics of this electrode. After the voltammetric oxidation in H_2SO_4, a decrease in I_p and an increase in ΔE_p and R_{ct} values was observed, which is associated with the formation of negatively charged oxidized groups on the electrode surface that interfere with the electron transfer processes of the probe anions in the electrode/solution interface (Jarocka et al., 2014; Dekanski et al., 2001). The electrostatic interactions between the positively charged AuNPs-SiPy nanohybrid and ox-GCE led to an increase in I_p and a decrease in R_{ct} values, which evidenced the immobilization of AuNPs on the electrode surface (Saha et al., 2012).

The CV of ox-GCE-[AuNPs-SiPy] resulted in a slightly lower oxidation current when compared to GCE-[SiPy]. This probably occurs because electron transport through the film is more difficult, due to the interaction between the redox probe with the AuNPs present in the nanohybrid. This hypothesis was confirmed when cationic $[Ru(NH_3)_6]^{2+/3+}$ complex was used in CV analysis. As observed in Fig. S3.5, the higher I_p (Table S3.2) was obtained because of lack of charge interaction.

3.3. Optimization steps of ZIKV DNA biosensor

The obtained ox-GCE-[AuNPs-SiPy] platform was then used for the immobilization of thiolate ssDNA-ZIKV1 (Au-S bond formation), followed by the hybridization with the target ssDNA-ZIKV2. The amount of AuNPs-SiPy deposited on ox-GCE, the incubation time of the electrodes in ZIKV1 ($time_{inc}$), the concentration of ZIKV1 solution and the temperature of ZIKV2 hybridization were optimized to favor the hybridization between probe and target ssDNA. These factors were analyzed by univariate or multivariate optimization processes. In all cases, higher ΔR_{ct} values evidenced a higher sensitivity of the proposed biosensor.

Firstly, the amount of AuNPs-SiPy was analyzed by a univariate process (n = 3), which showed an increase in ΔR_{ct} values until 5 µL and sequentially a decrease with the increase in the quantity of AuNPs-SiPy (Fig. S4.1). This result suggests that 5 µL is the most suitable amount of AuNPs-SiPy for biosensor construction.

[ZIKV1] and $time_{inc}$ were studied by a multivariate optimization process. The results obtained in the 3^2 full factorial design are shown in Table S4.1. The statistical processing of the experimental data indicates that [ZIKV1] and $time_{inc}$ had significant effects on the ΔR_{ct} response (at 95% confidence level). Moreover, the second-order interaction effect between both variables was statistically significant for obtaining a greater sensitivity of the biosensor (Fig. S4.2), suggesting that the variables influence the ΔR_{ct} response simultaneously. The results obtained from the 3^2 factorial design were fitted to a quadratic model, in which the response (ΔR_{ct}) is presented as a function of [ZIKV1] and $time_{inc}$. The resulting equation is:

$$\Delta R_{ct} = 287.47 - 32.815 \times (time_{inc})^2 - 38.94 \times ([ZIKV1])^2 + 9.44 \times time_{inc} \times [ZIKV1] - 3.42 \times time_{inc} \times ([ZIKV1])^2 + 2.94 \times (time_{inc})^2 \times [ZIKV1] + 13.80 \times (time_{inc})^2 \times ([ZIKV1])^2$$

The statistical validity of the obtained quadratic model was tested by applying analysis of variance (ANOVA), and the results are presented in Table S4.2. The model regression was statistically significant at 95% confidence level, and the variability explained by the model was very close to the maximum explainable variation ($R^2 = 0.9971$; Adj-$R^2 = 0.9927$). In addition, no lack of fit (LOF) could be identified ($F_{LOF} = 3.9 < F_{2,2,95\%} = 19.00$), which means that the proposed quadratic model had a good adjustment to the experimental data and was able to predict the behavior of the dependent variable (ΔR_{ct}) *versus* the studied independent variables ([ZIKV1] and $time_{inc}$) with a reliability of 99.3%.

The three-dimensional response surface plot corresponding to the quadratic model is shown in Fig. 1. In the experimental range studied for both variables, the ΔR_{ct} passes through a maximum, which corresponds to the optimal experimental region for the preparation of the ZIKV biosensor. The intense curvature represents the strong interaction between the variables, demonstrating that both factors affect the ΔR_{ct}. Therefore, the optimum conditions for the biosensor construction were: [ZIKV1] = 5.5 µmol L^{-1} and $time_{inc}$ = 120 min.

The temperature of hybridization between the ZIKV1 and ZIKV2 strands was optimized by a univariate process (n = 3). As the temperature increase provided higher ΔR_{ct} values (Fig. S4.3), 37 °C was chosen as the most suitable hybridization temperature since it allows maximum specificity without compromising sensitivity (Benvidi et al., 2015).

3.4. ZIKV DNA biosensor characterization

The optimized biosensor was characterized by CV and EIS (Fig. 2 (A) and (B)) (Table S5.1).

The ZIKV1 ssDNA probe immobilization on the ox-GCE-[AuNPs-SiPy] occurs by covalent Au-S bond formation, resulting in a decrease in I_p and increase of R_{ct} due to the insulating effect of the biomolecule (Dinçkaya et al., 2011). Since ZIKV1 contains disulfide bonds rather than free thiols, it was necessary to confirm that the binding of the ssDNA probe to the AuNPs-SiPy on the electrode surface could occur without the use of chemical pre-treatment (Wang et al., 2017). For this purpose, the immobilization of cystamine ($C_4H_{12}N_2S_2$) onto an ox-GCE-[AuNPs-SiPy] surface was performed (Fig. S5.1). The observed similarity in the increase of R_{ct} in this experiment provides the confirmation that covalent binding of ZIKV1 to AuNPs-SiPy occurs according to a parallel reaction. This new approach avoids the need to reduce the disulfide bonds of ZIKV1 ssDNA probe and the subsequent purification steps prior to application, making the construction of the present DNA biosensor faster, simpler and cheaper.

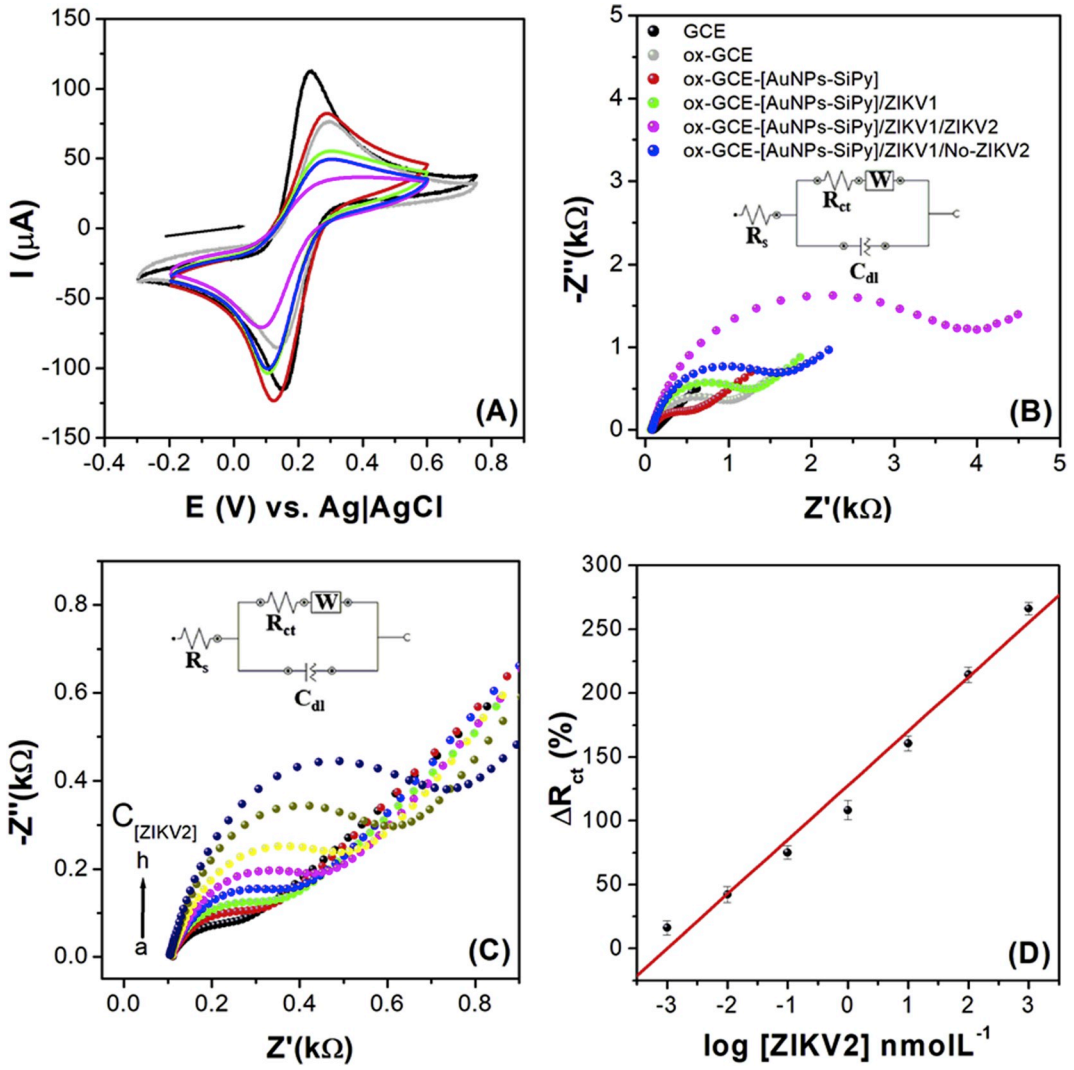

Fig. 2. (A) Cyclic voltammograms at 50.0 mV s^{-1} and (B) electrochemical impedance spectra of all steps of ZIKV biosensor construction, in 5 μmol L^{-1} of ZIKV1 and ZIKV2/No-ZIKV2. (C) Nyquist plots of GCE-[AuNPs-SiPy]/ZIKV1 after hybridization with different ZIKV2 concentrations: (a) 0.0, (b) 1.0 x 10^{-12} mol L^{-1}, (c) 1.0 x 10^{-11} mol L^{-1}, (d) 1.0 x 10^{-10} mol L^{-1}, (e) 1.0 x 10^{-9} mol L^{-1}, (f) 1.0 x 10^{-8} mol L^{-1}, (g) 1.0 x 10^{-7} mol L^{-1} and (h) 1.0 x 10^{-6} mol L^{-1}. (D) Analytical curve (n = 3). Experimental conditions: 0.15 mol L^{-1} PBS buffer solution (pH 7.4) with 5.0 mmol L^{-1} $K_4Fe(CN)_6/K_3Fe(CN)_6$; OCP; frequency range: 10.0 kHz to 0.1 Hz; amplitude: 10 mV.

The hybridization of ZIKV1, covalently bound to ox-GCE-[AuNPs-SiPy], with the ZIKV2 ssDNA target induced a decrease in I_p and an increase in R_{ct}, confirming the formation of dsDNA between probe and target ssDNA (Dinçkaya et al., 2011). In contrast, when ZIKV2 was replaced by No-ZIKV2 (no target ssDNA), no I_p and R_{ct} changes were observed in the last stage. These results indicate the specificity of the biosensor to ZIKV (Liu et al., 2010) and demonstrates that non-thiolate DNA does not significantly interact with the ox-GCE-[AuNPs-SiPy].

Besides R_{ct} and ΔR_{ct}, other important parameters (Table S5.1) obtained by EIS were also analyzed (Fig. 2 (B)). The resistance of the electrolyte, electrode and contacts (R_s) exhibits a slight increase during the stages of the biosensor construction, due to the insulating effect of the oligonucleotides. The double-layer capacitance (C_{dl}) from the constant-phase element (CPE) decreased, due to the smaller sensor/electrolyte interface area induced by oligonucleotide immobilization. The Warburg impedance (W) also decreased, which is related to the charge storage in the electrode. Due to the immobilization of the DNA sequences, the charge transfer process becomes more hindered and consequently the load of intercalated charge within the platform containing oligonucleotides decreases (Gonçalves et al., 2017).

3.5. Redox probe effect

In order to confirm that the interaction between the redox marker with the electrode surface does not significantly influence the electrode response (which could result in false-positive results), the ox-GCE-[AuNPs-SiPy] was incubated in the presence of $[Fe(CN)_6]^{4-/3-}$ instead of the oligonucleotides, with the same optimized $time_{inc}$ (120 min). The Nyquist diagram exhibits no significant increase in R_{ct} values, which indicates that the redox marker does not present a significant effect in the sensor response (Fig. S6.1).

3.6. AuNPs-SiPy influence

In order to justify the use of the AuNPs-SiPy for the covalent binding (S-Au) of the thiolate ZIKV1 ssDNA probe and for the biosensor response, a comparative study was carried out using three different configurations to hybridize the ZIKV2 ssDNA target: ox-GCE/ZIKV1, ox-GCE-[SiPy]/ZIKV1 and ox-GCE-[AuNPs-SiPy]/ZIKV1. After hybridization, the ΔR_{ct} values obtained for ox-GCE (8.6%) and ox-GCE-[SiPy] (47.4%) were significantly lower than those for ox-GCE-[AuNPs-SiPy] platform (277.8%) (Fig. S7.1). The higher R_{ct} values observed for ox-

GCE-[AuNPs-SiPy] occurs because, in the absence of AuNPs-SiPy, only unstable and weak interactions such as electrostatic and van der Waals could be established between the modified electrode and the immobilized ZIKV1 ssDNA probe, resulting in lower and non-reproducible ΔR_{ct} values. On the other hand, the use of AuNPs-SiPy provided a more effective immobilization of the thiolate ssDNA probe, enabling a more effective hybridization process with the ssDNA target (Austin et al., 2014).

3.7. Biosensor microscopy characterization

AFM images were obtained for each step of biosensor construction (Fig. S8.1). Ox-GCE revealed a smooth surface (Fig. S8.1(A)), while ox-GCE-[AuNPs-SiPy] presented a globular morphology (Fig. S8.1(B)), both being uniform. However, an increase in the roughness values (R_q) of ox-GCE (9.85 nm) to ox-GCE-[AuNPs-SiPy] (36.4 nm) was observed, proving the incorporation of the AuNPs-SiPy on the ox-GCE surface. After incubation in the presence of ZIKV1 ssDNA, a further increase of the R_q (54.8 nm) was observed (Fig. S8.1(C)), which is associated with the probe immobilization. The addition of ZIKV2 target to the system significantly increased the R_q values (95.8 nm), due to the formation of dsDNA (hybridization between ZIKV1 and ZIKV2 ssDNA), which is more elongated and less flexible than the ZIKV1 ssDNA probe (Fig. S8.1(D)) (De Castro et al., 2018; Oliveira et al., 2018). Finally, the hybridization with the No-ZIKV2 ssDNA target showed a lower increase of R_q (69.9 nm) (Fig. S8.1(E)), which can be attributed to the non-specific interaction with the ZIKV1 probe or the AuNPs-SiPy surface. The obtained images corroborate the results obtained by EIS: both R_q and R_{ct} values increased accordingly.

3.8. Analytical curve

Analytical curves for the ZIKV2 hybridization detection were obtained by EIS under the optimized conditions (Fig. 2 (C)), in which the concentration of ZIKV1 remained fixed in 5 μmol L^{-1} and the concentration of ZIKV2 target was varied from 1.0 x 10^{-12} to 1.0 x 10^{-6} mol L^{-1}. The increase in ZIKV2 concentration resulted in proportional increases in ΔR_{ct}, according to the linear regression equation: ΔR_{ct} (%) = 42.55 C_{ZIKV2} + 127.69, with R = 0.992 (Fig. 2 (D)).

The limit of detection (LOD) was determined following the IUPAC guidelines (Nic et al., 1997): LOD = 3 SD/b, where SD is the standard deviation of blank measurements (in the absence of any analyte; n = 3) and b is the slope of the analytical curve. The obtained LOD = 0.82 pmol L^{-1} suggested that ox-GCE-[AuNPs-SiPy] is a promising analytical platform for ZIKV detection. The DNA biosensor showed satisfactory sensitivity and LOD values (Table 1) in comparison to other techniques and platforms reported in the literature. Besides that, it presents additional advantages in comparison to other sensitive techniques presented in Table 1: namely, there is no need to synthesize cDNA or to buy expensive equipment, nor the need of the training time required by the LAMP method. Furthermore, there are no false-negatives or false-positive results, and the analysis time is shorter compared to the AG/AB serologic test. Although the work reported by Faria and Zucolotto (2019) shows interesting features such as portability and a simpler and disposable platform, we highlight that our sensor presents a lower assay time for the hybridization process, a wider linear range, a lower LOD (allowing the detection of ZIKV in biological fluids, Table S9.1) and no need of a chemical step to break the disulfide bond of the thiolate probe DNA oligonucleotides. Thus, it can be affirmed that the proposed DNA biosensor has the potential to efficiently and specifically quantify ZIKV, with a satisfactory analysis time and a lower cost.

3.9. Detection of ZIKV in serum and stability

The analytical performance of the presented DNA biosensor was also evaluated by the detection of ZIKV in human serum samples spiked

Table 1
Comparison of the developed DNA biosensor with reported sensors for ZIKV detection reported in the literature.

Platform	Assay technique	Detection strategy	Target	Linearity (mol L^{-1})	Detection limit (pmol L^{-1})	Assay Time (min)	Ref
ox-GCE-[AuNPs-SiPy]	VC, EIS	Electrochemical Label-free	DNA	1.0 $x10^{-12}$ –1.0 $x10^{-6}$	0.82	50	This work
Gold-PET	EIS, CV, DPV	Electrochemical Label-free	RNA (NS5)	54 $x10^{-9}$ – 340 $x10^{-9}$	25000	90	Faria and Zucolotto, (2019)
*FMR	LAMP	Colorimetry	DNA	7.8 $x10^{-12}$ – 250 $x10^{-12}$	1.0	40	Tian et al., (2018)
Graphene chips	EIS	Electrochemical Label-free	AB (NS1)	–	450	5	Afsahi et al., (2018)
3D Cu-based MOF [Cu(Dcbcp)(bpe)]$_n$	*F	Colorimetry	RNA	50 $x10^{-12}$ – 70 $x10^{-9}$	192	36	Xie et al., (2018)
*IDE- DTSP	EIS	Electrochemical Label-free	AB (NS1)	10 $x10^{-12}$ – 1.0 $x10^{-9}$	10	30	Kaushik et al., (2018)
IDE-GoxPol	VC, EIS	Electrochemical Label-free	Virus	5.2 $x10^{-20}$ – 5.2 $x10^{-15}$	1 x 10^{-8}	–	Tancharoen et al., (2018)

*FMR = ferromagnetic resonance,/*IDE-DTSP = gold interdigited electrode modified with dithiobis(succinimidyl propionate) (DTSP)/*F = fluorescence.

Table 2
Results for the detection of ZIKV in human serum samples using the ox-GCE-[AuNPs-SiPy]/ZIKV1 biosensor.

Serum samples	C_{ZIKV2} (nmol L^{-1}) added	ΔR_{ct} (%)	C_{ZIKV2} (nmol L^{-1}) detected
A	0.001	2.9	0.0011
B	1.0	128.0	1.02
C	1000.0	254.1	933.7

with different concentrations of ZIKV2 target. Despite the complex fluid composition, ZIKV2 was successfully detected from 10^{-6} to 10^{-12} mol L^{-1} (Table 2). Therefore, the biosensor is demonstrated to be an efficient and selective device for the detection of ZIKV in real clinical samples.

The stability of the proposed biosensor was also studied. The ox-GCE-[AuNPs-SiPy]/ZIKV1 were prepared, stored at 4 °C, and evaluated by EIS until hybridization detection. After each test, the biosensor was cleaned and another platform was constructed. This study showed that the sensor kept around 98.0% of its initial response after 90 days, as displayed in Fig. S10.1.

4. Conclusions

In this paper, a promising and sensitive impedimetric DNA biosensor based on a oxidized glassy carbon electrode modified with AuNPs-SiPy for detection of ZIKV is reported. Due to the high surface area and high electrical conductivity of the AuNPs, the loading amount of DNA probes was enhanced, resulting in a significantly improved electrochemical response of the developed biosensor. This proposed biosensing platform showed to be quite simple and appropriate for a suitable immobilization of ZIKV ssDNA probes (through the formation of Au-S covalent bonds), and was able to efficiently detect ZIKV in real human serum samples. The device demonstrated a suitable LOD of 0.82 pmol L^{-1} by EIS and exhibited stability for 90 days. The presented biosensor strategy can be further applied to the modification of disposable electrodes in order to make it commercially viable as a promising tool for ZIKV diagnosis in biological fluids.

Declaration of interests

The authors declare that they have no known competing financial interests or personal relationships that could have appeared to influence the work reported in this paper.

The authors declare the following financial interests/personal relationships which may be considered as potential competing interests:

CRediT authorship contribution statement

Marines Steinmetz: Conceptualization, Methodology, Validation, Formal analysis, Investigation, Writing - original draft. **Dhésmon Lima:** Conceptualization, Methodology, Formal analysis, Writing - original draft. **Adriano Gonçalves Viana:** Conceptualization, Methodology. **Sérgio Toshio Fujiwara:** Resources, Visualization. **Christiana Andrade Pessôa:** Conceptualization, Methodology, Writing - review & editing, Supervision. **Rafael Mazer Etto:** Conceptualization, Methodology, Investigation, Writing - review & editing, Supervision. **Karen Wohnrath:** Conceptualization, Methodology, Resources, Writing - review & editing, Supervision, Project administration, Funding acquisition.

Acknowledgements

The authors are grateful for financial support (grant and scholarship) from the Brazilian governmental agency Fundação Araucária (FA-SESA, grant number 073/2016 - CP 04/2016). We are also grateful to the Multi-User Laboratory Complex (C-Labmu/UEPG) and the to State University of Ponta Grossa (UEPG). We thank Cristiane Andrea Erdmann for the X-Rays analysis and Prof. R. T. Boeré (University of Lethbridge, AB, Canada) for the helpful suggestions on the final text. We also thank Microbial Molecular Biology Laboratory (LABMOM/UEPG) team for technical support.

Appendix A. Supplementary data

Supplementary data to this article can be found online at https://doi.org/10.1016/j.bios.2019.111351.

References

Afsahi, S., Lerner, M.B., Goldstein, J.M., Lee, J., Tang, X., Bagarozzi, D.A., Pan, D., Locascio, L., Walker, A., Barron, F., Goldsmith, B.R., 2018. Biosens. Bioelectron. 100, 85–88. https://doi.org/10.1016/j.bios.2017.08.051.
Alex, S., Tiwari, A., 2015. J. Nanosci. Nanotechnol. 15, 1869–1894. https://doi.org/10.1166/jnn.2015.9718.
Alfaya, R.V.S., Gushikem, Y., Alfaya, A.A., 1998. Processo de preparação do polieletrólito cloreto de 3-n-propilpiridínio ligado a uma estrutura de silsesquioxano. PI9803053-1.
Amorim, L., 2019. In: Shan, H., Dodd, R.Y. (Eds.), Zika Virus. Springer US, Stanford, pp. 163–186. https://doi.org/10.1007/978-3-319-94436-4.
Araujo, A.Q.C., Silva, M.T.T., Araujo, A.P.Q.C., 2016. Brain 139, 2122–2130. https://doi.org/10.1093/brain/aww158.
Austin, L.A., MacKey, M.A., Dreaden, E.C., El-Sayed, M.A., 2014. Arch. Toxicol. 88, 1391–1417. https://doi.org/10.1007/s00204-014-1245-3.
Bard, A.J., Faulkner, L.R., 2001. Electrochemical Methods: Fundamentals and Applications, second ed. John Wiley & Sons, New York.
Benvidi, A., Rajabzadeh, N., Mazloum-Ardakani, M., Heidari, M.M., 2015. Sensor. Actuator. B Chem. 673–682. https://doi.org/10.1016/j.snb.2014.10.043.
Brett, C.M.A., Brett, A.M.O., 1993. Electrochemistry: Principles, Methods, and Applications, first ed. Oxford University Press, Ney York.
Burke, L.D., Nugent, P.F., 1997. Gold Bull. 30, 43–53.
Cai, H., Xu, C., He, P., Fang, Y., 2001. J. Electroanal. Chem. 510, 78–85. https://doi.org/10.1016/S0022-0728(01)00548-4.
Calaça, G.N., Erdmann, C.A., Soares, A.L., Pessôa, C.A., Fujiwara, S.T., Garcia, J.R., Vidotti, M., Wohnrath, K., 2017. Electrochim. Acta 249, 104–112. https://doi.org/10.1016/j.electacta.2017.07.185.
Chao, J., Zhu, D., Zhang, Y., Wang, L., Fan, C., 2016. Biosens. Bioelectron. 76, 68–79. https://doi.org/10.1016/j.bios.2015.07.007.
Da Silva, P.S., Gasparini, B.C., Magosso, H.A., Spinelli, A., 2014. J. Hazard Mater. 273, 70–77. https://doi.org/10.1016/j.jhazmat.2014.03.032.
De Castro, A.C.H., Kochi, L.T., Moço, A.C.R., Coimbra, R.S., Oliveira, G.C., Cuadros-Orellana, S., Madurro, J.M., Brito-Madurro, A.G., 2018. J. Solid State Electrochem. 22, 2339–2346. https://doi.org/10.1007/s10008-018-3940-0.
De Menezes, E.W., Nunes, M.R., Arenas, L.T., Dias, S.L.P., Garcia, I.T.S., Gushikem, Y., Costa, T.M.H., Benvenutti, E.V., 2012. J. Solid State Electrochem. 16, 3703–3713. https://doi.org/10.1007/s10008-012-1782-8.
Dekanski, A., Stevanović, J., Stevanović, R., Nikolić, B.Ž., Jovanović, V.M., 2001. Carbon N. Y. 39, 1195–1205. https://doi.org/10.1016/S0008-6223(00)00228-1.
Deng, Y., Zhang, N., Li, X., Wang, Y., Tian, M., Qiu, Y., Fan, J., Hao, J., Huang, X., Dong, H., Fan, H., Wang, Y., Zhang, F., Tong, Y., Xu, Z., Qin, C., 2017. Nat. Commun. 8, 1–8. https://doi.org/10.1038/s41467-017-01923-4.
Dinçkaya, E., Kinik, Ö., Sezgintürk, M.K., Altuğ, Ç., Akkoca, A., 2011. Biosens. Bioelectron. 26, 3806–3811. https://doi.org/10.1016/j.bios.2011.02.038.
Dowall, S.D., Graham, V.A., Rayner, E., Hunter, L., Atkinson, B., Pearson, G., Dennis, M., Hewson, R., 2017. PLoS Neglected Trop. Dis. 11, 1–22. https://doi.org/10.1371/journal.pntd.0005704.
Faria, H.A.M., Zucolotto, V., 2019. Biosens. Bioelectron. 131, 149–155. https://doi.org/10.1016/j.bios.2019.02.018.
Gonçalves, R., Pereira, E.C., Marchesi, L.F., 2017. Int. J. Electrochem. Sci. 12, 1983–1991. https://doi.org/10.20964/2017.03.44.
Huang, Y., Xu, J., Liu, J., Wang, X., Chen, B., 2017. https://doi.org/10.3390/s17102375 17 1 30.
Jarocka, U., Sawicka, R., Góra-Sochacka, A., Sirko, A., Zagórski-Ostoja, W., Radecki, J., Radecka, H., 2014. Biosens. Bioelectron. 55, 301–306. https://doi.org/10.1016/j.bios.2013.12.030.
Kaushik, A., Yndart, A., Kumar, S., Jayant, R.D., Vashist, A., Brown, A.N., Li, C.Z., Nair, M., 2018. Sci. Rep. 8, 3–7. https://doi.org/10.1038/s41598-018-28035-3.
Kumarasamy, J., Camarada, M.B., Venkatraman, D., Ju, H., Dey, R.S., Wen, Y., 2018. Nanoscale 10, 1196–1206. https://doi.org/10.1039/c7nr06952a.
Liu, S., Liu, J., Wang, L., Zhao, F., 2010. Bioelectrochemistry 79, 37–42. https://doi.org/10.1016/j.bioelechem.2009.10.005.
Martinez, J.D., de la Garza, J.A.C., Cuellar-Barboza, A., 2019. Dermatol. Clin. 37, 95–105. https://doi.org/10.1016/j.det.2018.07.008.
Mashhadizadeh, M.H., Talemi, R.P., 2016. Mater. Sci. Eng. C 59, 773–781. https://doi.org/10.1016/j.msec.2015.10.082.
Mossanha, R., Erdmann, C.A., Santos, C.S., Wohnrath, K., Fujiwara, S.T., Pessoa, C.A., 2017. Sensor. Actuator. B Chem. 252, 747–756. https://doi.org/10.1016/j.snb.2017.06.001.
Musso, D., Gubler, D., 2016. Zika virus. Am. Soc. Microbiol. 11, 10–20. https://doi.org/

10.1128/CMR.00072-15 (Address).
Nic, M., Jirat, J., Kosata, B., 1997. Compendium of Chemical Terminology - IUPAC Gold Book [WWW Document]. Blackwell Sci. Publ. https://doi.org/10.1351/goldbook.
Oliveira, D.A., Silva, J.V., Flauzino, J.M.R., Castro, A.C.H., Moço, A.C.R., Soares, M.M.C.N., Madurro, J.M., Brito-Madurro, A.G., 2018. Anal. Biochem. 549, 157–163. https://doi.org/10.1016/j.ab.2018.03.023.
Pardee, K., Green, A.A., Takahashi, M.K., Braff, D., Lambert, G., Lee, J.W., Ferrante, T., Ma, D., Donghia, N., Fan, M., Daringer, N.M., Bosch, I., Dudley, D.M., O'Connor, D.H., Gehrke, L., Collins, J.J., 2016. Cell 165, 1255–1266. https://doi.org/10.1016/j.cell.2016.04.059.
Petersen, L.R., Jamieson, D.J., Powers, A.M., Honein, M.A., 2016. N. Engl. J. Med. 374, 1552–1563. https://doi.org/10.1056/NEJMra1602113.
Rafique, B., Iqbal, M., Mehmood, T., Shaheen, M.A., 2018. Sens. Rev. https://doi.org/10.1108/SR-08-2017-0156.
Saha, K., Agasti, S., Kim, C., Li, X., Rotello, V., 2012. Chem. Rev. 112, 2739–2779. https://doi.org/10.1021/cr2001178.
Singh, R.K., Dhama, K., Karthik, K., Tiwari, R., Khandia, R., Munjal, A., Iqbal, H.M.N., Malik, Y.S., Bueno-Marí, R., 2018. Front. Microbiol. 8, 1–17. https://doi.org/10.3389/fmicb.2017.02677.
Tancharoen, C., Sukjee, W., Thepparit, C., Jaimipuk, T., Auewarakul, P., Thitithanyanont, A., Sangma, C., 2018. ACS Sens. 4 acssensors.8b00885. https://doi.org/10.1021/acssensors.8b00885.
Tian, B., Liao, X., Svedlindh, P., Strömberg, M., Wetterskog, E., 2018. ACS Sensors. https://doi.org/10.1021/acssensors.8b00048.
Wang, L., Veselinovic, M., Yang, L., Geiss, B.J., Dandy, D.S., Chen, T., 2017. Biosens. Bioelectron. 87, 646–653. https://doi.org/10.1016/j.bios.2016.09.006.
Wang, Y., Laborda, E., Crossley, A., Compton, R.G., 2013. Phys. Chem. Chem. Phys. 2, 3133–3136. https://doi.org/10.1039/c3cp44615h.
Xie, B.-P., Qiu, G.-H., Hu, P.-P., Liang, Z., Liang, Y.-M., Sun, B., Bai, L.-P., Jiang, Z.-H., Chen, J.-X., 2018. Sensor. Actuator. B Chem. 254, 1133–1140. https://doi.org/10.1016/j.snb.2017.06.085.
Zhang, N., Zhang, N., Qin, C.F., Liu, X., Shi, L., Xu, Z., 2016. Cell Stem Cell 19, 120–126. https://doi.org/10.1016/j.stem.2016.04.017.